Title

Restoration of visual function by expression of a light-gated mammalian ion channel in retinal ganglion cells or ON-bipolar cells

Journal

Proceedings of the National Academy of Sciences of the United States of America, 111(51)

ISSN

0027-8424

Authors

Gaub, Benjamin M
Berry, Michael H
Holt, Amy E
et al.

Publication Date

2014-12-23

DOI

10.1073/pnas.1414162111

Peer reviewed

Restoration of visual function by expression of a light-gated mammalian ion channel in retinal ganglion cells or ON-bipolar cells

Benjamin M. Gaub[a,1], Michael H. Berry[b,1], Amy E. Holt[b], Andreas Reiner[b], Michael A. Kienzler[b], Natalia Dolgova[c], Sergei Nikonov[d], Gustavo D. Aguirre[c], William A. Beltran[c], John G. Flannery[a,b,e,2], and Ehud Y. Isacoff[a,b,f,2]

[a]Helen Wills Neuroscience Institute, and Departments of [b]Molecular and Cell Biology and [e]Optometry, University of California, Berkeley, CA 94720; [c]Section of Ophthalmology, Department of Clinical Studies, School of Veterinary Medicine, University of Pennsylvania, Philadelphia, PA 19104; [d]Department of Neuroscience, Perelman School of Medicine, University of Pennsylvania, Philadelphia, PA 19104; and [f]Physical Bioscience Division, Lawrence Berkeley National Laboratory, Berkeley, CA 94720

Edited* by Carla J. Shatz, Stanford University, Stanford, CA, and approved November 3, 2014 (received for review July 25, 2014)

Most inherited forms of blindness are caused by mutations that lead to photoreceptor cell death but spare second- and third-order retinal neurons. Expression of the light-gated excitatory mammalian ion channel light-gated ionotropic glutamate receptor (LiGluR) in retinal ganglion cells (RGCs) of the retina degeneration (*rd1*) mouse model of blindness was previously shown to restore some visual functions when stimulated by UV light. Here, we report restored retinal function in visible light in rodent and canine models of blindness through the use of a second-generation photoswitch for LiGluR, maleimide-azobenzene-glutamate 0 with peak efficiency at 460 nm ($MAG0_{460}$). In the blind *rd1* mouse, multielectrode array recordings of retinal explants revealed robust and uniform light-evoked firing when LiGluR-$MAG0_{460}$ was targeted to RGCs and robust but diverse activity patterns in RGCs when LiGluR-$MAG0_{460}$ was targeted to ON-bipolar cells (ON-BCs). LiGluR-$MAG0_{460}$ in either RGCs or ON-BCs of the *rd1* mouse reinstated innate light-avoidance behavior and enabled mice to distinguish between different temporal patterns of light in an associative learning task. In the rod-cone dystrophy dog model of blindness, LiGluR-$MAG0_{460}$ in RGCs restored robust light responses to retinal explants and intravitreal delivery of LiGluR and $MAG0_{460}$ was well tolerated in vivo. The results in both large and small animal models of photoreceptor degeneration provide a path to clinical translation.

retinal gene therapy | visual prosthetics | retinitis pigmentosa | optogenetic pharmacology | azobenzene photoswitches

Inherited retinal degenerative diseases affect 1 in 3,000 humans worldwide (1). Retinitis pigmentosa (RP) describes a family of over 50 different gene mutations that cause progressive loss of rod photoreceptors (1, 2). Rod loss is followed by degeneration of cone photoreceptors, ultimately leading to complete blindness in many patients (3). Despite the complete loss of photoreceptors in the outer nuclear layer, many interneurons of the inner retina survive in a functional state for long periods, providing an opportunity for treatment (4, 5).

Direct electrical stimulation of the surviving inner retina has proven to be successful in restoring useful vision (6–8). One approach employs surgically implanted photovoltaic or electrode arrays to stimulate retinal ganglion cells (RGCs) (8) or bipolar cells (BCs) (6, 7) directly in the inner nuclear layer (INL) of the degenerated retina, and promising results in clinical trials have led to US Food and Drug Administration approval for the Argus II device (Second Sight Medical Products, Inc.) (8). The electrical implants demonstrate that inner retinal neurons in blind patients can respond to appropriate stimulation and lead to a useful visual percept allowing simple navigation and object recognition. These electronic designs are under continual development to increase the resolution, improve the surgical implantation procedures, and increase the sophistication of their signal-encoding algorithms (9).

Microbial opsins, like channelrhodopsin and halorhodopsin, have been successfully tested as visual prosthetics in animal models of human blindness (10–15). Genetically encoded light-gated proteins can be exogenously expressed in retinal cells using viral or nonviral gene delivery vehicles, imparting a light-sensitive function to cone photoreceptors that have become insensitive to light from loss of their outer segments (14), but also to ON-BCs (12, 13), as well as RGCs (10, 15, 16), leading to rescue of basic aspects of visual function in mice. Microbial opsins are appealing for this application due to the bioavailability of the light-sensitive ligand retinal. However, there are potential drawbacks to this approach. Xenotransplantation is generally concerning, because it might lead to immune responses and inflammation potentially spreading to the brain via the optic nerve.

Significance

We restored visual function to animal models of human blindness using a chemical compound that photosensitizes a mammalian ion channel. Virus-mediated expression of this light sensor in surviving retinal cells of blind mice restored light responses in vitro, reanimated innate light avoidance, and enabled learned visually guided behavior. The treatment also restored light responses to the retina of blind dogs. Patients that might benefit from this treatment would need to have intact ganglion cell and nerve fiber layers. In general, these are patients diagnosed with retinitis pigmentosa and some forms of Leber congenital amaurosis. Patients diagnosed with other types of blindness, for example, age-related macular degeneration or diabetic retinopathy, would not be candidates for this treatment.

Author contributions: B.M.G., M.H.B., A.E.H., A.R., G.D.A., W.A.B., J.G.F., and E.Y.I. designed research; B.M.G., M.H.B., A.E.H., A.R., N.D., and S.N. performed research; M.A.K. contributed new reagents/analytic tools; B.M.G., M.H.B., and A.R. analyzed data; B.M.G., M.H.B., A.R., M.A.K., G.D.A., W.A.B., J.G.F., and E.Y.I. wrote the paper; and J.G.F. and E.Y.I. supervised the project. M.A.K. synthesized the $MAG0_{460}$ photoswitch. A.R. performed HEK cell experiments and established the intensity dependence of $MAG0_{460}$. B.M.G. performed intraocular AAV injections and retinal histology in mice. B.M.G. and M.H.B. performed mouse MEA recordings and data analysis. B.M.G., M.H.B., A.E.H., performed mouse behavior testing. M.H.B., N.D., S.N., and W.A.B. performed canine MEA recordings and data analysis. G.D.A. and W.A.B. performed intraocular AAV injections and ophthalmic eye examinations in dogs. N.D. and W.A.B. performed retina histology in dogs.

Conflict of interest statement: E.Y.I. is an author on US Patent US 8,114,843 B2 on the design of protein photoswitches and a cofounder of Photoswitch Biosciences, Inc., which employs such switches in cell-based assays for drug screening and is developing an alternative method for restoration of vision that employs noncovalent photoswitches which endow light sensitivity onto native channels.

*This Direct Submission article had a prearranged editor.

[1]B.M.G. and M.H.B. contributed equally to this work.

[2]To whom correspondence may be addressed. Email: flannery@berkeley.edu or ehud@berkeley.edu.

This article contains supporting information online at www.pnas.org/lookup/suppl/doi:10.1073/pnas.1414162111/-/DCSupplemental.

Additionally, once expressed, it is impossible to silence the system in case of adverse reactions in patients.

One promising alternative to microbial opsins is an optopharmacological strategy that uses synthetic azobenzene-based photoswitches to endow light sensitivity either to native ion channels of neurons (17, 18) or to engineered mammalian receptors and channels that, like the microbial opsins, allow for genetic targeting to specific cells (19–22). We previously showed that an engineered light-gated ionotropic glutamate receptor (LiGluR) restores light responses to blind retina degeneration (*rd1*) mice (23). The gene encoding for LiGluR was delivered to RGCs by intravitreal injection of adeno-associated virus (AAV), and the photoswitchable tethered ligand maleimide-azobenzene-glutamate (MAG) was delivered in a subsequent intravitreal injection (23). LiGluR contains a single Cys substitution in the kainate receptor, *GluK2(439)C*, which serves as an anchoring site for MAG close to the ligand binding site. Upon illumination at 380 nm in the near-UV range, the azobenzene linker in MAG photoisomerizes from *trans* to *cis,* shortening the molecule and allowing the glutamate to bind into the ligand binding pocket to activate and open the channel.

The first-generation MAG photoswitch suffered from two major limitations for vision restoration: (*i*) The UV light needed for activation is absorbed by the human lens and can damage the retina, and (*ii*) MAG is bistable, requiring a second pulse of light at a longer wavelength for deactivation. We recently developed a second-generation photoswitch, maleimide-azobenzene-glutamate 0 with peak efficiency at 460 nm ($MAG0_{460}$), to overcome these problems (24). $MAG0_{460}$ is activated by white light and spontaneously turns off in the dark. In the present study, we compare retinal light responses and both innate and learned visually guided behaviors in the *rd1* mouse model of retina degeneration when LiGluR-$MAG0_{460}$ is targeted to either RGCs or ON-BCs. We find that both cell types support robust light-induced retinal activity and visually guided behavior. To demonstrate efficacy in a larger animal model, we targeted LiGluR-$MAG0_{460}$ to RGCs in a canine model of human blindness and restored light-activated retinal responses in vitro. Because LiGluR-$MAG0_{460}$ is functional in both the mouse and dog, it is an attractive candidate for a genetically encoded retinal prosthetic for the blind.

Results

Restoration of Light Response to the Retina of the *rd1* Mouse by LiGluR in RGCs or ON-BCs. Our first-generation MAG photoswitch for LiGluR had limited utility for vision restoration because it required 380-nm UV light stimulation for activation and a second pulse of light at a longer wavelength for deactivation (19, 25). We therefore turned to a recently developed second-generation compound, $MAG0_{460}$, which is activated by blue or white light and spontaneously turns off in the dark (Fig. 1). Expression and labeling in human embryonic kidney (HEK) cells yielded robust LiGluR-$MAG0_{460}$ photocurrents that were stable and reversible over hundreds of switching cycles (24). Importantly, LiGluR-$MAG0_{460}$ photocurrents scaled with light intensity, yielding a sigmoid intensity-response curve spanning three orders of magnitude (Fig. 1*D*, Fig. S1, and *SI Text*). In addition, LiGluR responded dynamically to moderate frequencies of intensity modulation (Fig. S1 *C* and *D*).

We tested the expression and function of LiGluR-$MAG0_{460}$ in the retina of the *rd1* mouse, a small animal model of human blinding disease. The *rd1* mouse has a null mutation in the phosphodiesterase type 6 (*PDE6*)-beta subunit causing complete loss of rod and cone photoreceptors by postnatal day 90 (p90) (26). This phenotype is comparable to patients in the early stages of retinal degeneration who may still have a functioning network of all retinal cell types except for the photoreceptors. At later stages, however, only the RGCs may survive (4, 27). To address both early and late stages of the disease, we examined the effect of targeting LiGluR to either the RGCs or ON-BCs (Fig. 2 *C* and *E*).

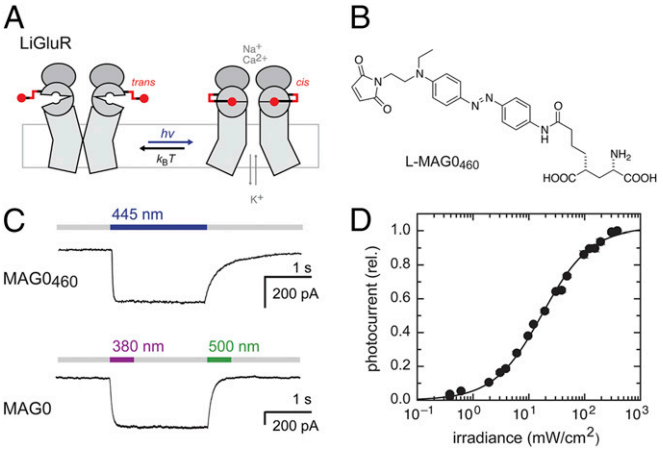

Fig. 1. LiGluR-$MAG0_{460}$ expressed in HEK cells is activated by visible light, relaxes in the dark, and detects changes in light intensity. (*A*) Schematic of the LiGluR. After tethering a photoswitchable ligand, L-$MAG0_{460}$, the channel is activated by light and closes in darkness. (*B*) Structural formula of the second-generation L-$MAG0_{460}$ photoswitch (24). *hv*, frequency × Planck constant; k_BT, Boltzmann constant × temperature. (*C*) HEK cell recordings in voltage-clamp configuration at −75 mV. (*Top*) LiGluR conjugated with $MAG0_{460}$ is activated by blue light and relaxes spontaneously in the dark. (*Bottom*) For comparison, LiGluR gating with the first-generation MAG0 photoswitch, which is bistable (380 nm of light opens the channel, 500 nm of light closes it), is shown. (*D*) Dynamic range of LiGluR-$MAG0_{460}$ with respect to light intensity. LiGluR-$MAG0_{460}$ responds over a wide range of intensities (0.5–500 mW/cm^2 or 1.1×10^{15} photons per cm^{-2}·s^{-1} to 1.1×10^{18} photons per cm^{-2}·s^{-1}) with a sigmoid intensity-response profile (normalized steady-state currents, mean ± SD, $n = 3$ experiments). rel., relative. Details are provided in Fig. S1 and *SI Text*.

Good restriction of LiGluR expression in RGCs was achieved using an AAV vector combining the human synapsin promoter (*hsyn-1*) and the AAV 2/2 capsid as previously described (23). The gene expression cassette (Fig. 2*A*) in a volume of 2 μL containing 10^9–10^{10} viral genomes was injected into the vitreous of *rd1* mice. Expression was visualized >4 wk after injection using an antibody against the *GluK2* subunit from which LiGluR is composed (19). Intravitreal injection of the vector resulted in expression in the RGC layer (Fig. 2 *D* and *G* and Fig. S2*A*). Due to the limited retinal penetration of the AAV2/2 serotype (15) and the lack of *syn-1* expression in choline acetyltransferase-positive amacrine cells (28), these transduced cells are likely to be predominantly RGCs. LiGluR expression was panretinal and localized to soma and dendrites of both ON- and OFF-RGCs, as seen by stratification of the dendritic terminals in both on- and off-sublayers of the inner plexiform layer (IPL) (Fig. 2*G* and Fig. S2*A*).

Targeting ON-BCs required the use of an AAV capsid with deeper tissue penetration and an ON-BC–specific promoter. To achieve deeper penetration, we turned to the tyrosine mutant AAV2/2 capsids (29), which are protected from proteasome degradation, leading to better transduction in the inner retina. We restricted LiGluR expression to ON-BCs with a four-copy concatemer of a minimal version of the cell-specific metabotropic glutamate receptor 6 promoter (*mGluR6*) promoter (*4xgrm6*) (12, 30). This gene expression cassette (Fig. 2*B*) was packaged into AAV2/2(4YF) (29) and injected subretinally in *rd1* mice (1–2 mo old), creating a bleb covering ∼25% of the retinal surface (Fig. S2*B*). Subretinal injections were used instead of intravitreal injections because this route enabled us to deposit the AAV closer to the ON-BC target cells. Expression was confirmed >6 wk after virus injection by staining with the anti-*GluK2* antibody, and it was predominantly found in ON-BCs, as seen by stratification of the

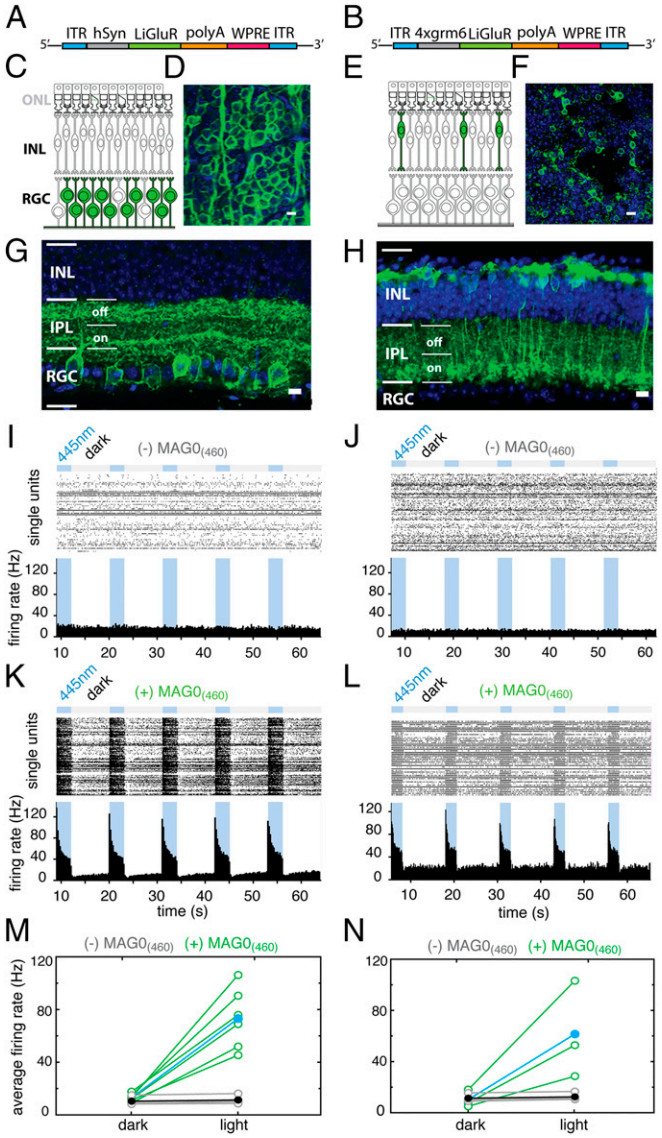

Fig. 2. LiGluR expression downstream in RGCs and upstream in ON-BCs restores light responses in the *rd1* mouse retina in vitro (light intensity for all recordings: 27.7 mW/cm^2 or 6.3 × 10^{16} photons per cm^{-2}·s^{-1}). (*A* and *B*) Viral DNA expression cassette. LiGluR is flanked by inverted terminal repeat (ITR) domains and stabilized by a polyadenylation signal sequence (*polyA*) and a woodchuck hepatitis posttranscriptional regulatory element (*WPRE*). ONL, outer nuclear layer. LiGluR expression is driven by *hsyn-1* (*A*) or *4xgrm6* (*B*). (*C* and *E*) Schematic of a degenerated *rd1* mouse retina with targeted cells highlighted in green. Confocal images of LiGluR expression in RGCs of *rd1* mouse retina >4 wk after intravitreal injection of AAV2/2-hSyn-LiGLuR (2-μL volume equal to 5 × 10^{11} viral genomes) (*D* and *G*) or ON-BCs of *rd1* mouse retina >6 wk after subretinal injection of AAV2/2-(4YF)-4xgrm6-LiGLuR (2-μL volume equal to 5 × 10^{11} viral genomes) (*F* and *H*). Retinas were stained with an anti-*GluK2* antibody (green), and nuclei were stained with DAPI (blue). (Scale bars: 10 μm.) The IPL is shown with indication of on- and off-sublayers. MEA recordings from *rd1* mouse retinas expressing LiGluR in RGCs (*I* and *K*) or ON-BCs (*J* and *L*) in the absence (*I* and *J*) or presence (*K* and *L*) of MAG0$_{460}$. (*Top*) Light stimulation protocol: 5× 3 s of blue light and 8 s dark. (*Middle*) Raster plot with spikes for all light-sensitive RGCs (*I* and *K*, $n = 130$ cells; *J* and *L*, $n = 46$ cells). (*Bottom*) Peristimulus time histogram (PSTH) with 250-ms bins. Comparison of the average firing rates (500-ms bins) in the light vs. dark for *rd1* retinas expressing LiGLuR in RGCs (*M*) and ON-BCs (*N*) in the absence (gray) (*M*: $n = 6$ retinas, 478 cells; *N*: $n = 4$ retinas, 416 cells) and presence (green) (*M*, $n = 5$ retinas, 303 cells; *N*, $n = 4$ retinas, 332 cells) of MAG0$_{460}$ and population mean (black and blue, respectively).

axon terminals in the on-sublayer of the IPL in the area under the bleb (Fig. 2 *F* and *H* and Fig. S2*B*).

Retinal explants from *rd1* mice (>3 mo old) were mounted on a 60-channel multielectrode array (MEA) to test light-evoked activity. Aside from a small fraction of sluggish, intrinsically photosensitive RGCs, retinas from untreated *rd1* mice showed no blue light-induced firing (Fig. S2*E*), consistent with the absence of rods and cones. Incubation of untreated *rd1* retina with 100 μM MAG0$_{460}$ followed by washout left them unresponsive to blue light (Fig. S2*F*). In contrast, *rd1* retinas expressing LiGluR in RGCs, which were insensitive to blue light (Fig. 2*I*), showed strong light-induced firing following exposure to MAG0$_{460}$ (Fig. 2 *K* and *M*). Similarly, *rd1* retinas expressing LiGluR in ON-BCs were insensitive to blue light (Fig. 2*J*) until they were exposed to MAG0$_{460}$ (Fig. 2 *L* and *N*). Stimulation with broad-spectrum (white) light triggered similar responses (Fig. S2*G*), as demonstrated previously in HEK cells (24). Both in RGCs and ON-BCs, LiGluR-MAG0$_{460}$ was able to drive light responses at moderate intensities (0.3 mW/cm^2 or 7.1 × 10^{14} photons per cm^{-2}·s^{-1} for RGCs and 0.2 mW/cm^2 or 4.7 × 10^{14} photons per cm^{-2}·s^{-1} for ON-BCs, respectively, Fig. 3 *A* and *B*), representing an ∼10-fold improvement in sensitivity compared with the published values for the first-generation MAG photoswitch (23).

Kinetics and Frequency Detection Supported by Light-Sensitive RGCs and ON-BCs. Ideally, a visual prosthetic should have low variability, elicit RGC firing similar to wild-type (wt) conditions, and show fast dynamics to restore natural vision after loss of photoreceptor cells (31–33). LiGluR-MAG0$_{460}$ expressed in ON-BC and RGC showed low cell-to-cell variability (Fig. S3) similar to wt retinas. The firing rate above baseline (Fig. S3*A*) and the type of response (Fig. S3*B*) to a full-field flash of light was comparable. This was also true for retina-to-retina variability (Fig. S4 and Table S1) measured in vitro. We found that light pulses as short as 35 ms in duration were sufficient to trigger robust RGC firing when LiGluR-MAG0$_{460}$ was expressed in either RGCs or ON-BCs (Fig. 3 *C* and *D*). In both cases, the responses reached a peak firing rate similar to the peak firing rate observed with much longer pulses of light (compare Fig. 2 *K* and *L* with Fig. 3 *C* and *D*).

The responses had a short delay following light onset and terminated rapidly from peak response to baseline as shown by the decay constant tau (τ) (τ_{off} = 51.96 ms, SEM = 3.48 with LiGluR-MAG0$_{460}$ in RGCs; τ_{off} = 62.87 ms, SEM = 5.26 with LiGluR-MAG0$_{460}$ in ON-BCs), with values from steady state to baseline [LiGluR-MAG0$_{460}$ in RGCs: response inactivation time (ΔT_{off}) = 40 ms (Fig. S5*C*), LiGluR-MAG0$_{460}$ in ON-BCs: ΔT_{off} = 80 ms (Fig. S5*D*)]. The similarity between RGC-driven (Fig. 3*C* and Fig. S5*C*) and ON-BC–driven (Fig. 3*D* and Fig. S5*D*) termination suggests that the decay kinetics are mostly governed by ligand inactivation from the *cis* to *trans* state, and the speed (Fig. 3 *C* and *D*) suggests that these systems should enable retinal output to follow high-frequency modulation of light intensity. We tested this hypothesis by measuring RGC firing in response to trains of short light pulses given at either 4 Hz (50-ms flashes at a 200-ms interstimulus interval) or 10 Hz (50-ms flash with a 50-ms interstimulus interval) with LiGluR-MAG0$_{460}$ in RGCs (Fig. 3 *E* and *G*) or in ON-BCs (Fig. 3 *F* and *H*). In both cases, at 4 Hz, the individual RGCs responded to every flash of light. With increasing frequency, the light-induced firing rate decreased (Fig. S5*B*) and individual cells stochastically missed some responses (Fig. S5*A*). At the population level, however, *rd1* retinas with LiGluR-MAG0$_{460}$ in RGCs and ON-BCs reliably followed 4-Hz (Fig. 3 *E* and *F*) and 10-Hz stimulation frequencies (Fig. 3 *G* and *H*). LiGluR-MAG0$_{460}$ elicited graded changes in the RGC firing rate in response to graded changes in light intensity (Fig. S5*G*) similar to what we saw in HEK cells (Fig. S1*C*).

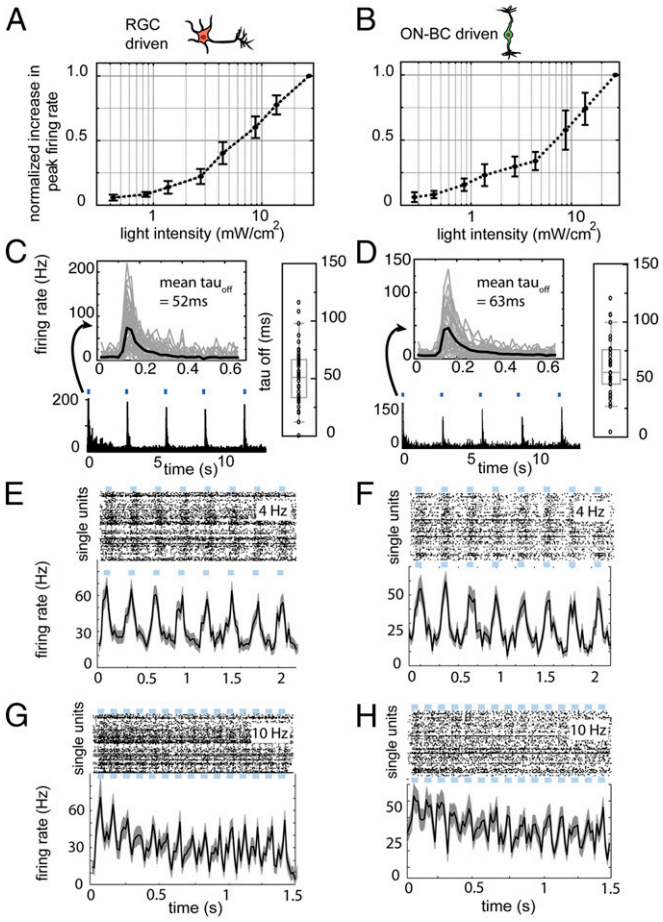

Fig. 3. LiGluR-MAG0$_{460}$ in RGCs and ON-BCs of *rd1* mouse retina drives light responses with similar characteristics (other than for *A* and *B*, light intensity for all recordings is 24.7 mW/cm^2 or 5.6 × 10^{16} photons per cm^{-2}·s^{-1}). (*A–H*) MEA recordings of *rd1* mouse retinas treated with LiGluR-MAG0$_{460}$ in RGCs (*Left*) or ON-BCs (*Right*). (*A* and *B*) Dynamic range with 3-s stimulation (*A*: $n = 4$ retinas, 287 cells; *B*: $n = 4$ retinas, 150 cells). Data are mean ± SD. (*C* and *D*) Responses to brief (35-ms) flashes of light. (*Insets*) Responses of single cells in gray (*C*, $n = 47$ cells; *D*, $n = 33$ cells) and population average in black with mean τ_{off}. All traces were fit exponentially, and the time constants for the peak decay reflecting MAG0$_{460}$ dark relaxation are shown as scatter plots and summarized in a box plot. (*E–H*) LiGluR responses to frequency-modulated stimulation (50-ms flashes) (*E*, $n = 77$ cells; *F*, $n = 67$ cells; *G*, $n = 70$ cells; *H*, $n = 65$ cells). (*Top*) Raster plots showing indication of light flashes in blue and single-unit spikes in black (500-ms bins). (*Bottom*) PSTHs showing population averages of all single-cell responses to 4 Hz and 10 Hz of stimulation in black, with a gray shadow indicating the standard error (SEM).

Differences Between Light-Induced RGC Firing with LiGluR in RGCs vs. ON-BCs. More than 20 different subtypes of RGCs have been classified in the mouse retina to date based on physiology and morphology, including dendritic stratification and input pathways (34, 35). Some of the synaptic connections in the INL are maintained in early stages of degeneration (5, 36). Engaging those synaptic connections through LiGluR expression in ON-BCs may lead to diverse light responses in the downstream RGCs, indicating that aspects of RGC identity might be retained or restored. In contrast, bypassing these synaptic connections by LiGluR expression in RGCs themselves should lead to uniform responses across all LiGluR-RGCs regardless of their original identity (e.g., ON vs. OFF, transient vs. sustained).

To explore our hypothesis in vitro using the MEA, we examined single-unit RGC responses to 1-s flashes of light for four different conditions: wt (Fig. 4*A*), *rd1* LiGluR-MAG0$_{460}$ in either RGCs (Fig. 4*B*) or ON-BCs (Fig. 4*C*), and *rd10* LiGluR-MAG0$_{460}$ in ON-BCs (Fig. 4*D*). Nonpatterned light was used as a stimulus to allow comparisons to be made without concern for variability of LiGluR expression levels and density (compare Fig. 2 *D* and *F* and Fig. S2 *A* and *B*). Peristimulus time histograms (PSTH) were plotted for each recording (Fig. 4 *E–H*). In *rd1* mice, RGCs with LiGluR-MAG0$_{460}$ showed uniform responses, with similar onset delays and decay rates (Fig. 4 *B* and *F*). The photoswitching index (PI; normalized difference in firing rates in the light vs. dark) was positive for every cell (Fig. 4*F*) as expected for its direct excitation by LiGluR-MAG0$_{460}$. In contrast, *rd1* RGCs that received synaptic input upstream from ON-BCs with LiGluR-MAG0$_{460}$ showed more diverse responses (Fig. 4*C*). Some cells were excited by light, and others were inhibited (Fig. 4 *C* and *G*). The onset, offset, and duration of the light response also varied among cells (Fig. 4*C*) similar to wt retina (Fig. 4 *A* and *E*).

The diversity of responses seen in single units prompted us to ask if this effect could be seen more globally at the level of the retina, taking into account all of the cells from one recording. Rather than averaging across cells, and thus masking cell-to-cell variation, we wanted to analyze all responses systematically from each cell individually to understand the relationship between the RGC firing patterns generated by LiGluR-MAG0$_{460}$ installed in the RGCs themselves or in the ON-BCs. To this end, we correlated the PSTH (the firing rate of a given cell over time) of all cells with one another and constructed a correlation matrix in which each data point represents the correlation value (r). Responses during the 1-s light flash and responses 100 ms before

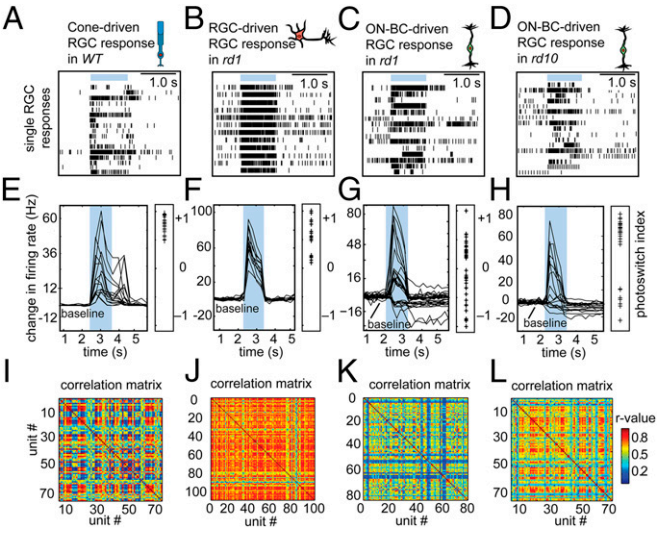

Fig. 4. LiGluR expression downstream in RGCs synchronizes responses, and LiGluR expression upstream in ON-BCs diversifies responses from the *rd1* mouse in vitro (light intensity for all recordings: 24.7 mW/cm^2 or 5.6 × 10^{16} photons per cm^{-2}·s^{-1}). MEA data from wt retina (*A*, *E*, and *I*), *rd1* retina treated with LiGluR-MAG0$_{460}$ in RGCs (*B*, *F*, and *J*) or ON-BCs (*C*, *G*, and *K*), and *rd10* retina treated with LiGluR-MAG0$_{460}$ in ON-BCs (*D*, *H*, and *L*) are shown. (*A–D*) Representative raster plots of RGC responses to a 1-s flash of light (*A*, $n = 17$; *B*, $n = 12$; *C*, $n = 15$; *D*, $n = 17$ cells). (*E–H*) Representative traces from single units in response to 1-s light flashes (*D*, $n = 16$; *E*, $n = 14$; *F*, $n = 28$; *G*, $n = 17$ cells; 250-ms bins). The blue bar indicates the light flash. The light responses are quantified by calculating the PI (normalized firing rate light-dark; *E*, $n = 20$; *F*, $n = 17$; *G*, $n = 57$; *H*, $n = 29$ cells). Positive values indicate an increase in firing rate, and negative values indicate a decrease in firing rate in response to light. (*I–L*) Correlation matrices showing correlations between all light-sensitive single units. RGC responses during the 1-s flash and 100 ms immediately before and after the flash were used for the correlation. The color of the heat map indicates the magnitude of the correlation value r, with warmer colors indicating higher values (*I*, $n = 72$ cells; *J*, $n = 111$ cells; *K*, $n = 82$; *L*, $n = 76$ cells).

and after the flash were used to construct the correlation matrices. Heat maps represent the correlation score, with warm colors representing high correlation values. Using this unbiased and inclusive analysis, we confirmed that LiGluR-MAG0$_{460}$ in RGCs leads to uniform responses across all cells (Fig. 4*J* and Fig. S6 *B* and *C*), whereas LiGluR-MAG0$_{460}$ in ON-BCs yielded overall lower correlation in RGC output (Fig. 4*K* and Fig. S6 *B* and *C*). The wt retinas with photoreceptor-driven activity showed low levels of correlation (Fig. 4*I* and Fig. S6*B*) as expected due to the functional diversity of RGCs. The ON-BC–LiGluR–MAG0$_{460}$ correlation matrix showed a higher diversity of responses and shared more similarity with wt retinas than with retinas that have LiGluR-MAG0$_{460}$ in RGCs. LiGluR-MAG0$_{460}$ in ON-BCs of the *rd10* mouse retina, which undergoes slower retinal degeneration, also showed higher levels of diversity or low levels of correlation (Fig. 4 *D*, *H*, and *L* and Fig. S6*B*) similar to LiGluR-MAG0$_{460}$ installed in ON-BCs of the *rd1* mouse retina, indicating that the effect we observed was specific to the different target cells and not a function of retinal degeneration.

LiGluR Restores Innate and Learned Associative Light-Guided Behavior. We next asked whether LiGluR-MAG0$_{460}$ could restore basic visually guided behavior. Mice naturally avoid brightly lit open spaces (37). This preference is absent in adult *rd1* mice that have lost all rod and cone photoreceptors (14, 16). To test for restoration of light avoidance, we placed wt mice and *rd1* mice with LiGluR in RGCs or ON-BCs in an open field test (Fig. 5*A*) and tested their behavior before and after treatment with MAG0$_{460}$. Mice were first habituated to the testing environment, which consisted of an open-topped plastic box with dark and light compartments connected by a small opening (Fig. 5*A*), and then allowed to explore the box for 5 min. The percentage of time spent in the light compartment was recorded (16). Following intravitreal injection of MAG0$_{460}$, mice with LiGluR in RGCs ($n = 18$) or ON-BCs ($n = 13$) showed a strong light avoidance, which was similar to the light avoidance of wt mice ($n = 4$) (Fig. 5*B*).

After establishing that we can restore light avoidance behavior, we asked how long the restoration of the light response would last following a single intravitreal injection of MAG0$_{460}$ as the receptor protein on the cell surface turns over. Following a single intravitreal injection of MAG0$_{460}$ in *rd1* mice expressing LiGluR in RGCs, the light-induced firing of RGCs in isolated retinas was found to decline with a time constant of ~9 d (τ = 8.8 d) (Fig. 5*C*). The behavioral preference for the dark compartment declined over a similar time course following a single intravitreal injection of MAG0$_{460}$ (Fig. 5*D*).

Because LiGluR-MAG0$_{460}$ targeted to either RGCs or ON-BCs can restore the ability of blind mice to distinguish light from dark, we wanted to test whether it would also enable animals to distinguish temporal patterns of light and use this information in the context of a learned behavior. Based on our finding that LiGluR-MAG0$_{460}$ can follow moderate frequencies of intensity modulation (Fig. 3 *E* and *F*), we created two visual stimuli of identical intensity, with the cue stimulus flashing at a rate of 2 Hz and the decoy stimulus emitting light of constant intensity. These visual stimuli were presented in a radial arm water maze that was modified into a forced two-choice task (Fig. 5*E*). Mice were first habituated to the maze and then trained to associate a specific light cue with a hidden escape platform (38) for 8 d at 20 trials per day. These conditions were chosen to maximize exposure of mice to this task within the efficacy period of a single treatment with MAG0$_{460}$, as determined by the open field test (Fig. 5 *C* and *D*). A correct trial was defined as a mouse finding the platform in under 1 min without exploring the wrong arm of the maze first.

We used four groups of mice for this study: wt mice (positive control), *rd1* mice expressing LiGluR in RGCs or ON-BCs and injected intravitreally 24 h prior to day 1 with MAG0$_{460}$ (experimental), and *rd1* mice that were sham-injected (negative control). The wt mice ($n = 6$) performed well, improved gradually, and were able to learn the task ($P < 0.016$) within 8 d (Fig. 5*F* and Fig. S7*A*), in agreement with earlier studies (38). The performance of sham-injected *rd1* mice ($n = 8$) did not improve ($P = 0.815$) over the 8-d experiment (Fig. 5*F* and Fig. S7*B*). In contrast, *rd1* mice with LiGluR-MAG0$_{460}$ in either RGCs ($n = 9$) or ON-BCs ($n = 6$) learned to distinguish the temporally patterned stimulus from the decoy stimulus ($P < 0.0025$ and $P < 0.017$, respectively) (Fig. 5*F* and Fig. S7 *C* and *D*). The light intensities used for the light avoidance and water maze tasks were 7 mW/cm^2 or 1.6 × 10^{16} photons per cm^{-2}·s^{-1} and 5 mW/cm^2 or 1.1 × 10^{16} photons per cm^{-2}·s^{-1}, respectively, which correspond to outdoor light levels on a sunny day (approximation in Fig. S8).

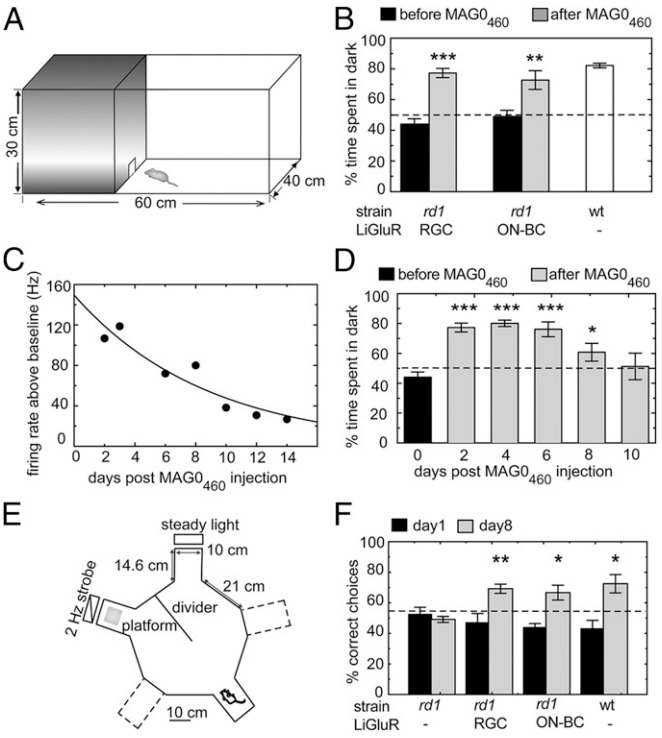

Fig. 5. LiGluR expression restores innate and learned light-guided behavior in *rd1* mice in vivo. (*A*) Schematic showing the light/dark box for the open field test. (*B*) Percentage of time spent in the dark compartment plotted before (black) and after (gray) administration of MAG0$_{460}$ for *rd1* RGC-LiGluR ($n = 18$), *rd1* ON-BC–LiGluR ($n = 13$), and wt mice ($n = 4$). Data are mean ± SEM. $^{**}P < 0.005$, $^{***}P < 0.0005$; paired Student *t* test (light intensity: 7 mW/cm^2 or 1.6 × 10^{16} photons per cm^{-2}·s^{-1}). (*C*) Biological $t_{1/2}$ of intravitreally injected MAG0$_{460}$. RGC-LiGluR–expressing *rd1* mice were injected with a single dose of MAG0$_{460}$ in vivo 24 h before day 1. Subsequently, on days 2–14, retinal explants were prepared and responses to 3-s flashes were plotted. The decay of LiGluR-MAG0$_{460}$–induced light responses was fit with an exponential curve decay constant τ = 8.75 ± 0.79 d. (*D*) Efficacy of MAG over time in vivo. RGC-LiGluR–expressing *rd1* mice ($n = 7$) from *B* were tested over the course of 10 d. The percentage of time spent in the dark compartment is plotted for *rd1* RGC-LiGluR mice before MAG0$_{460}$ ($n = 18$) and for *rd1* RGC-LiGluR mice after receiving a single intravitreal dose of MAG0$_{460}$ at day 2 ($n = 18$), day 4 ($n = 7$), day 6 ($n = 7$), day 8 ($n = 7$), and day 10 ($n = 7$). Data are mean ± SEM. $^{*}P < 0.01$, $^{***}P < 0.0001$; multiple *t* tests with Bonferroni correction. (*E* and *F*) Forced two-choice associative learning task with a modified radial arm maze. (*E*) Schematic of the maze with dimensions given in centimeters. (*F*) Performance of the four groups of mice on day 1 (black) vs. day 8 (gray). Percentage of correct choices is plotted for sham (PBS)-treated *rd1* mice [–LigluR, –MAG0$_{460}$ ($n = 8$); *rd1* RGC-LiGluR + MAG0$_{460}$ ($n = 9$); *rd1* ON-BC–LiGluR + MAG0$_{460}$ ($n = 6$); and wt mice ($n = 6$)]. Data are mean ± SEM. $^{*}P < 0.05$, $^{**}P < 0.005$, paired Student *t* test (light intensity at the divider 5 mW/cm^2 or 1.1 × 10^{16} photons per cm^{-2}·s^{-1}).

LiGluR in RGCs Restores the Retinal Light Responses in a Canine Model of Retinal Blindness. Next, we wanted to confirm that the LiGluR-MAG_{460} system could be virally delivered and drive functional light responses in a larger animal model. To assess whether LiGluR-$MAG0_{460}$ is effective in a human-sized eye, we expanded our study to the canine model, which provides both anatomical and pathological similarities that are clinically relevant for testing retinal therapies (39). The rod-cone dystrophy (*rcd1*) model has a nonsense mutation in *PDE6B,* the same gene that is defective in the *rd1* and *rd10* mice. We used an AAV2/2(4YF) vector in combination with the ubiquitous cytomegalovirus CMV promoter variant *CAG* to deliver the LiGluR transgene to RGCs (Fig. 6 *A* and *B*). Intravitreal injection of AAV2/2(4YF)-CAG-LiGluR in the area centralis, a region of high RGC density in the canine retina (40), resulted in potent expression in RGCs by 8 wk post-injection (Fig. 6 *C* and *D*).

MEA recordings were performed in three degenerated retinas from two mutant *rcd1* dogs that had been intravitreally injected 8–11 wk earlier with AAV2/2(4YF)-CAG-LiGluR. Stimulation with high-intensity (75 mW/cm^2 or 1.7×10^{17} photons per cm^{-2}·s^{-1}) blue light in the absence of $MAG0_{460}$ did not alter the baseline RGC firing activity (Fig. 6*E*). However, following 20 min of incubation in 100 μM $MAG0_{460}$ and thorough washout, strong and repeated periods of light-induced firing were seen that peaked shortly after the onset of light (Fig. 6 *F* and *G*). To explore the sensitivity of LiGluR-$MAG0_{460}$ to photopic light levels typically encountered within the brightly illuminated working/living environment of humans, we performed MEA recordings in the *rcd1* canine retina at different levels of blue light ranging from 6.8 to 0.43 mW/cm^2 or 1.5×10^{16} photons per cm^{-2}·s^{-1} to 9.7×10^{14} photons per cm^{-2}·s^{-1}, respectively. Light stimulations (1-s duration) induced RGC firing that was still detectable at the lowest (0.43 mW/cm^2 or 9.7×10^{14} photons per cm^{-2}·s^{-1}) irradiance and increased with higher intensities (Fig. 6*H*). Responses to all five intensities had a transient component and a sustained component, and showed similar kinetics with rapid inactivation time from steady-state to baseline levels (40 ms) upon offset of light (Fig. 6*I*).

To develop future psychophysical tests to be used in dogs and human patients for the assessment of visual function recovery after intervention with LiGluR-$MAG0_{460}$, we examined the response of the retina to a combination of higher frequency (4 Hz), shorter duration (50 ms), and low light intensity (0.85 mW/cm^2 or 1.9×10^{15} photons per cm^{-2}·s^{-1}) stimulations. Whereas peak firing rate was reduced and a slight delay was introduced in comparison to responses achieved with longer stimulations at higher intensities, a distinct light-induced ON response of RGCs that peaked at the end of the 50-ms stimulation period could be detected (Fig. 6*J*). Rapid relaxation of the photoswitch ($\tau_{off} \approx$ 28 ms) occurred upon returning to darkness (Fig. 6*J*, *Inset*).

Discussion

In this study, we show the translational potential of the LiGluR-$MAG0_{460}$ system for retinal gene therapy to cure human blindness. In a mouse model of the human retinal degenerative disease RP, we observed restoration of a useful retinal output in response to light when LiGluR was expressed either in the most upstream or the most downstream cell types that survive after photoreceptor degeneration. In vivo, these retinal responses restored an innate light-guided behavior and enabled light-associated learning based on cues with distinct temporal patterns.

Earlier work validated the use of LiGluR in conjunction with a first-generation MAG0 photoswitch in RGCs for vision restoration (23). However, the therapeutic utility of the first-generation MAG0 was limited by two properties. First, the spectral sensitivity of the original MAG0 chromophore was outside of the visible range, peaking in the UV light at 380 nm (41), which penetrates the lens poorly and is damaging to corneal, lens epithelial, and retinal cells. Second, LiGluR-MAG0 was bistable,

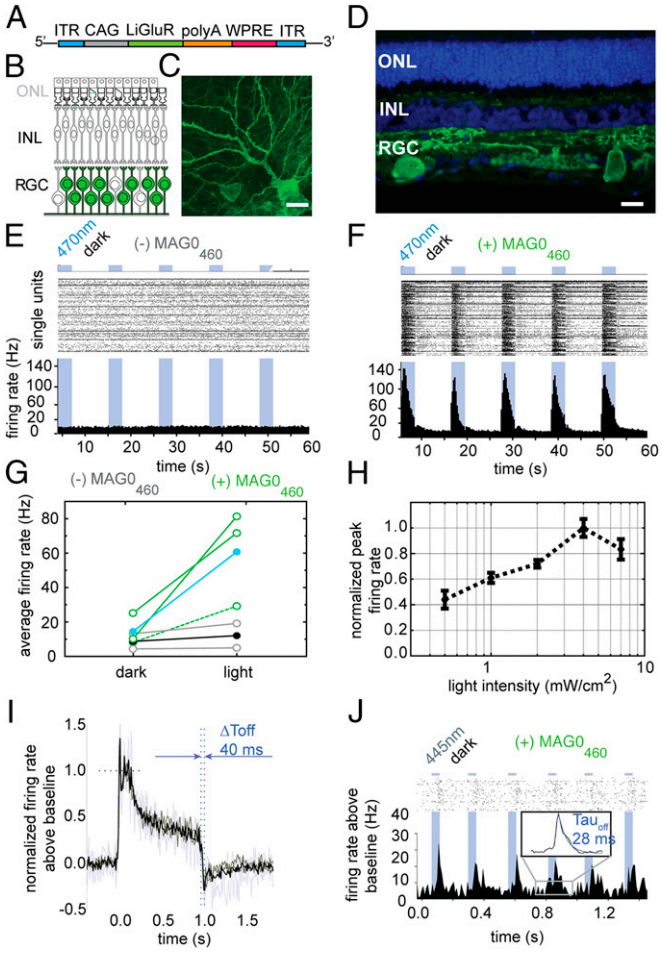

Fig. 6. LiGluR expression in RGCs restores light responses in the *rcd1* canine retina in vitro. (*A*) Viral DNA expression cassette. LiGluR expression is driven by *CAG* promoter. (*B*) Schematic of degenerated canine retina with targeted RGCs in green. (*C* and *D*) Confocal images of LiGluR expression in canine retina 8 wk after intravitreal injection of AAV2/2 (4YF)-CAG-LiGluR. (Scale bars: 20 μm.) (*C*) Whole-mount view of LiGluR expression in RGCs of *rcd1* canine retina. (*D*) Cross-section of LiGluR expression in RGCs of wt canine retina. (*E–J*) MEA recordings (light intensity: 75 mW/cm^2 or 1.7×10^{17} photons per cm^{-2}·s^{-1} if not specified otherwise) of *rcd1* mutant canine retinas. MEA recording from an *rcd1* mutant dog expressing LiGluR ($n = 160$ cells) before (*E*) and after (*F*) in vitro application of $MAG0_{460}$. (*G*) Comparison of the firing rate averaged over a 3-s flash of light (500-ms bins) on three LiGluR-expressing *rcd1* retinas in the dark vs. light (dashed line, 6.8 mW/cm^2 or 1.5×10^{16} photons per cm^{-2}·s^{-1}; solid lines, 75 mW/cm^2 1.7×10^{17} photons per cm^{-2}·s^{-1}) before ($n = 2$ retinas, 193 cells, gray) and after ($n = 3$ retinas, 291 cells, green) in vitro application of $MAG0_{460}$, with population means (black and blue, respectively). (*H*) Dynamic range of *rcd1* retina treated with LiGluR-$MAG0_{460}$ at lower light conditions ($n = 80 \pm 5$ cells). Data are mean ± 2 SEM binned at 100 ms. (*I*) Averaged normalized response to stimulation with five light intensities (0.43, 0.85, 1.7, 3.4, and 6.8 mW/cm^2 or 9.7×10^{14}, 1.9×10^{15}, 3.8×10^{15}, 7.7×10^{15}, and 1.5×10^{16} photons per cm^{-2}·s^{-1}, respectively) shown in *H* with individual responses shown in gray, average response over all intensities shown in black, and the response inactivation time shown in blue (ΔT_{off}). (*J*) MEA recording from an *rcd1* retina treated with LiGluR and $MAG0_{460}$ ($n = 77$ cells) stimulated at low intensity (0.85 mW/cm^2 or 1.9×10^{15} photons per cm^{-2}·s^{-1}) at 4 Hz (50-ms duration, 200-ms ISI) binned at 10 ms. (*Inset*) Average of 400 individual responses (5-ms bins) with a single exponential fit (blue trace) and time constant ($\tau_{off} \sim 28$ ms) for $MAG0_{460}$ relaxation from peak response to baseline.

requiring a second longer wavelength pulse of light to reset the system after each activating event (19, 41), which would necessitate additional hardware for potential clinical applications. We solved these problems with our photoswitch, $MAG0_{460}$,

which is activated by blue light similar to blue cone photoreceptors, responds well to broad-spectrum visible light, and rapidly and spontaneously turns off in the dark (24). LiGluR-MAG0$_{460}$ responds dynamically to incremental changes in light intensity and supports reliable retinal output with intensity modulations at moderate frequencies of 4–10 Hz.

We compared two gene therapy target cell types, RGCs and ON-BCs, for LiGluR-MAG0$_{460}$ expression in the degenerating mouse retina. RGCs are well-suited therapy targets for late-stage disease because they have been shown to stay morphologically intact (4) with minimal remodeling following photoreceptor degeneration compared with the other retinal cells (27). Furthermore, RGCs are easily targeted due to their proximity to the vitreous, enabling strong, uniform, and widespread expression after intravitreal injection of AAV vectors. ON-BCs, however, are promising therapeutic targets for early-stage disease because they are located upstream in the retinal circuit and provide an opportunity to preserve aspects of retinal processing (32, 33).

Robust light responses were restored to the RGCs of retinas isolated from blind mice when LiGluR-MAG0$_{460}$ was installed in either the RGCs themselves or in ON-BCs. The sensitivity, ability to follow frequency-modulated light, and on/off kinetics in response to full-field illumination were similar for the two cell types. The similarity is striking considering that expression was much sparser after viral delivery to the ON-BCs (compare Fig. S2 *A* and *B*). Comparable sensitivity at lower expression suggests that the signal amplification due to convergence from BCs to RGCs (42) makes the ON-BC population particularly effective for vision restoration and highlights the value of further improvement for gene delivery to these cells.

There was an important distinction between the properties of the restored retinal output activity when LiGluR-MAG0$_{460}$ was installed in the two cell types. In *rd1* mouse ON-BCs, LiGluR-MAG0$_{460}$ drove RGC activity that was temporally diverse and excited a subset of RGCs, whereas other RGCs were inhibited by light. In contrast, LiGluR-MAG0$_{460}$ in *rd1* mouse RGCs led to uniform light responses, as one would expect from direct excitation of the RGCs. The signal diversity that emerges from the retinal circuit when LiGluR-MAG0$_{460}$ is installed in ON-BCs could be beneficial for restoring critical aspects of visual processing, such as contrast and edge detection (43). Single-unit RGC responses from ON-BC LiGluR-MAG0$_{460}$ in both *rd1* and *rd10* resembled the RGC responses seen in wt retina more closely than RGC LiGluR-MAG0$_{460}$. ON-BCs might therefore be the target of choice in early stages of retinal degeneration, before substantial synaptic remodeling has occurred (27). In late stages of retinal degeneration with severe circuit degeneration, it may be preferable to target the least affected cells, the RGCs, to generate a strong and synchronized output signal.

We tested the function of LiGluR-MAG0$_{460}$ in vivo and found that the restored retinal activity supported normal light-avoidance behavior in blind treated mice using the open field test. Having established that our treatment supported light-guided behavior, we next asked whether the LiGluR-MAG0$_{460}$ system would enable blind mice to learn to distinguish different visual cues in the context of a forced two-choice variant of the Morris water maze task. In this experiment, mice were challenged to associate a temporally patterned cue stimulus from a non-patterned intensity-matched decoy stimulus. The wt mice were able to learn to associate the patterned stimulus with the reward, whereas untreated *rd1* mice were not and did not improve their performance over the 8 d of the experiment. *Rd1* mice treated with LiGluR-MAG0$_{460}$ in either the RGCs or ON-BCs learned to perform as well as wt animals, indicating that the LiGluR-MAG0$_{460}$ system operates as more than just a mere light meter and can inform mice about qualitative aspects of the visual world. In this study, we did not attempt to record visually evoked potentials, record electroretinograms, or test for a pupillary light reflex as we did for our previous study (23). Instead, we focused our efforts on learned associations and demonstrated the ability of mice to recognize temporal patterns in the water maze task. We have not yet tested these mice for spatial pattern recognition or temporal and spatial pattern resolution.

Our results in the mouse model encouraged us to test if our treatment could be translated to a larger animal model. Specifically, we set out to test virus-mediated expression of the LiGluR receptor and the ability of LiGluR-MAG0$_{460}$ to drive light responses in retinal explants. To this end, we selected the *rcd1* dog, which, like the *rd1* mouse, has severe and early-onset rod and cone degeneration (44, 45). We developed a virus for canine RGC transduction and tested patches of retina collected from the area centralis region for LiGluR-MAG0$_{460}$–induced light responses in vitro. LiGluR-MAG0$_{460}$ in the RGCs rendered the blind dog retina light-sensitive, with characteristics closely matching the characteristics observed in the *rd1* mouse. Our results show that the LiGluR-MAG0$_{460}$ system in excised *rcd1* canine retina responds well to stimulation at a light intensity found under natural environmental conditions [0.43 mW/cm^2, which approximates outdoor conditions (Fig. S8)] and moderate frequencies (up to 4 Hz). These findings pave the way for future efforts in the canine model to determine toxicity and a therapeutic index for the MAG0$_{460}$ photoswitch and to perform behavioral testing in advanced retinal degeneration.

A recent study restored the ability to distinguish light from dark using just a chemical photoswitch that acts on native ion channels, including those native ion channels that are up-regulated in the RGCs of the degenerating mouse retina (17). Compared with this optochemical therapy, which has advantages of not requiring gene transfer and being more sensitive to light (comparison of threshold light intensities in Fig. S8), our two-component optochemical-genetic therapy has the advantage of designed cell-type targeting. In addition, covalent attachment of the chromophore allows us to work at lower concentrations of the photoswitch chemical, a factor that, along with targetability, could provide a better safety profile. In both the optochemical and optochemical-genetic therapy approaches, a bolus supply of the photochemical restores light-guided behavior temporarily for a period of days. In the optochemical case, the limited efficacy is presumably due to washout of the molecule, whereas in our optochemical-genetic case, it is most likely due to turnover of the photoswitch-conjugated receptor. As a result, both of these approaches would benefit from sustained-release drug delivery technology.

An alternative purely optogenetic approach has proven successful for restoration of light responses in retinal cells, light responses in visual cortex, light aversion, and learned association tasks using unpatterned light. For this approach, microbial opsins are expressed in specific cell types of the degenerated retina from cone cell bodies that have lost their outer segment to ON-BCs and RGCs (10, 13, 14, 16). The simplicity of this genetic therapy is appealing, as is the ability of the microbial opsins to use the retina's supply of 11-cis-retinal as the natural photoswitch. One concern about this approach is the possibility of an immune response to the foreign protein, which, in the worst case scenario, could spread into the brain via the optic nerve. In addition, once expressed, these opsins cannot be turned off in case of an adverse reaction. Our success with a mammalian light-gated protein that is identical in amino acid sequence to the native protein, except for a single amino acid substitution that creates the photoswitch anchoring site, reduces the risk of immune reaction. In addition, the dependence on chronic delivery of the synthetic photoswitch should make it possible to discontinue treatment in case of an adverse reaction as well as to replace the synthetic photoswitch with improved photoswitches as they become available.

In summary, we have shown that the LiGluR-MAG0$_{460}$ system operates successfully in either ON-BCs, at the upstream end of the degenerating retina, or at the output end of the retina, in RGCs, to restore retinal light responses and enable innate and

learned light-guided behavior in blind mice. Installation in the ON-BCs, which is probably most appropriate for early-stage degeneration, provides more diverse retinal output characteristics and may support higher quality vision, a notion that will require future testing. Importantly, the system is equally effective in the *rcd1* dog in vitro, paving the way for extensive testing of high-resolution vision in a preclinical setting and for clinical development. Our approach should allow for the use of a receptor protein based on the patient's own receptor, reducing the chance of an immune response. Because the functional properties of the restored light response depend on the externally provided photoswitch, it can be tailored to the patient and improved as new photoswitches become available; equally importantly, the function of the system can be aborted in case of adverse effects by curtailing photoswitch delivery.

Methods

Animals. All mouse experiments were performed with approval of the University of California Animal Care and Use Committee. The wt mice (C57BL/6J) and *rd1* mice (C3H) were purchased from the Jackson Laboratory and housed on a 12-h light/dark cycle with food and water ad libitum. The age of the mice ranged from p30–p60 for rAAV injections and from p90–p160 for in vivo and in vitro experiments.

All experiments on dogs were approved by the Institutional Animal Care and Use Committee of the University of Pennsylvania and were carried out in strict accordance with the recommendations in the *Guide for the Care and Use of Laboratory Animals* of the NIH (46) and with the US Department of Agriculture's Animal Welfare Act and Animal Welfare Regulations, and complied with the Association for Research in Vision and Ophthalmology Statement for the Use of Animals in Ophthalmic and Vision Research. Three *rcd1* dogs (*PDE6B* mutation) (47) with late-stage retinal degeneration (0.4, 1.8, and 3.7 y of age) and one normal dog (2.4 y of age) were used to assess viral vector tropism and for MEA experiments (details are provided below).

Injection of rAAV and MAG Photoswitch. AAVs were produced via standard methods (48). We selected rAAV2/2 carrying the LiGluR transgene under the control of the *hsyn-1* promoter for RGC targeting. For ON-BC targeting, we selected rAAV2/2(4YF) carrying the LiGluR transgene under the control of the 4x repeat of the *mGluR6* promoter (*4xgrm6*), a kind gift from Botond Roska (Friedrich Miescher Institute, Basel) and Connie Cepko (Harvard Medical School, Boston). The titer of AAV was determined via quantitative PCR relative to the inverted terminal repeat domains standard. Titers for these viruses ranged between 1×10^{13} viral genomes (vg)/mL and 1×10^{14} vg/mL. Mice were anesthetized with i.p. ketamine (72 mg/kg) and xylazine (64 mg/kg). Eyes were additionally anesthetized with proparacaine (0.5%), and pupils were dilated with phenylephrine (2.5%) and tropicamide (1%). Injections consisted of a two-step process. First, an incision was made posterior of the ora serrata using a sharp 30-gauge needle. Then, a 2-μL volume of $MAG0_{460}$ photoswitch diluted in PBS/DMSO or an estimated amount of 5×10^{11} viral genomes of AAV diluted in PBS (with 1% phenol red as a contrast agent) was injected intravitreally for rAAV2/2-hsyn-LiGluR or subretinally for rAAV2/2(4YF)-4xgrm6-LiGluR using a blunt 32-gauge Hamilton syringe. Efflux was minimized by keeping the Hamilton needle tip in the eye for >60 s.

Intravitreal injections in dogs were performed under general gas (isofluorane) anesthesia. A 150-μL volume of rAAV2/2 (4YF) carrying the GFP reporter gene under the control of the ubiquitous *CAG* promoter was delivered intravitreally (preretinally) to the superior/tapetal fundus region of a 20-wk-old mutant *rcd1* dog using a 39-gauge polyimide cannula (RetinaJet; SurModics, Inc.). The right eye was injected with a viral titer of 1.46×10^{11} vg/mL, whereas the contralateral (left) eye received a 10-fold higher viral titer (1.46×10^{12} vg/mL). At 12 wk postinjection, expression of GFP was assessed by noninvasive retinal imaging using a scanning confocal laser ophthalmoscope (HRA/OCT; Heidelberg Engineering) set on the autofluorescence mode. Following euthanasia, the eyes were processed for immunohistochemistry as stated below and localization of GFP expression to retinal cell populations was examined. Subsequently, an AAV2/2(4YF)-CAG-LiGluR viral construct was produced and injected preretinally to the area centralis region of one normal and the two *rcd1* mutant dogs. The rAAV was diluted in balanced salt solution (Alcon Laboratories), and 200 μL of two viral titers (1.46×10^{11} vg/mL and 5×10^{11} vg/mL) was injected.

MAG Preparation. A stock solution of 100 mM $MAG0_{460}$ (L-diastereomer) (24) in 100% pharmaceutical grade DMSO (Cryoserv; Bioniche Pharma) was diluted 1:100 in sterile PBS for a final working solution of 1 mM in 1% DMSO. Working solutions were prepared immediately before administration and were used within 20 min to avoid hydrolysis of the maleimide group. In vitro conjugation of $MAG0_{460}$ on retinal explants for electrophysiological recordings was performed in a volume of 200 μL at a concentration of 100 μM $MAG0_{460}$ (in PBS with >1% DMSO). For in vivo experiments and the MAG efficacy experiment (Fig. 5), a 2-μL volume of 1 mM $MAG0_{460}$ solution (in PBS with 1% DMSO) was injected into eyes that had been treated with AAV >6 wk earlier. In dogs, 1 mL of 100 μM $MAG0_{460}$ (in Ringer's solution) was applied to the retinal explants for MEA recordings.

Tissue Preparation and Immunohistochemistry. Mice were killed >4 wk (for RGC-LiGluR) or >6 wk (for ON-BC–LiGluR) post-AAV injection, and the eyes were enucleated and fixed in 4% paraformaldehyde (Ted Pella) for 1 h. Whole-mount retinas were prepared by making a complete circular incision around the ora serrata using scissors, removing the cornea while leaving the lens attached, gently tearing the eyecup apart using two forceps, and finally removing the lens. Radial cuts were made to flatten the retina, resulting in the typical cloverleaf shape. For retinal sections, whole mounts were embedded in agarose (Sigma) and sectioned transverse using a vibratome (Leica Microsystems) at medium speed, maximum vibration, and 150-μm thickness. Whole mounts and vibratome sections were incubated in blocking buffer [10% normal goat serum, 1% BSA, 0.5% Triton X-100 in PBS (pH 7.4)] for 2 h at room temperature (RT). Monoclonal antibody against *GluK2/K3* (Millipore) was applied at a 1:500 dilution in blocking buffer overnight at 4 °C. Secondary anti-rabbit Alexa 488 or Alexa 594 antibody (Invitrogen) was applied at a 1:1,000 dilution in blocking buffer for 2 h at RT. Tissue was washed three times for 10 min with PBS and mounted on slides using Vectashield (Vector Laboratories) mounting medium with DAPI to stain cell nuclei. Whole mounts and sections were imaged via confocal microscopy (LSM7; Carl Zeiss). To identify off-target cell expression outside of the expected layer, we prepared a total of 44 vibratome sections from four treated retinas from three mice [previously injected with AAV2/2-hsyn-LiGluR or AAV2/2(4YF)-4xgrm6-LiGluR] and counted the number of labeled cell bodies outside of the RGC layer or the IPL, respectively. In dogs, ocular tissues were collected following i.v. injection of a euthanasia solution (Euthasol; Virbac). Retinal tissues used for immunohistochemistry on retinal cryosections or whole mounts were processed as previously reported (40) and examined by confocal microscopy (Leica TCS SP5; Leica Microsystems).

HEK Cell Recordings. HEK 293T cells were transfected with an LiGluR expression vector [pcDNA-*GluK2*(Q) L439C] using Lipofectamine 2000 (Invitrogen) and YFP as a transfection marker (24, 49) Cells were labeled after expression for 24–48 h at 37 °C. Cells were washed with external solution, incubated for 2 min with 0.3 mg/mL Con A to block ligand-induced desensitization, and labeled with ~25 μM $MAG0_{460}$ or regular MAG0 (19) for 40 min in extracellular solution at RT in the dark. After labeling, any unreacted MAG was removed by thorough washing with external solution. Whole-cell HEK cell recordings were performed in voltage-clamp configuration, typically at −75 mV, on an inverted microscope (Olympus IX) using an Axopatch 200B head stage/amplifier (Molecular Devices) at 22–24 °C. Patch pipettes were pulled from borosilicate glass to give 3–7 MΩ resistance when filled with internal solution [135 mM K-gluconate, 10 mM NaCl, 10 mM Hepes, 2 mM $MgCl_2$, 2 mM MgATP, 1 mM EGTA (pH 7.4)]. The extracellular solution was 138 mM NaCl, 1.5 mM KCl, 1.2 mM $MgCl_2$, 2.5 mM $CaCl_2$, 10 mM glucose, and 10 mM Hepes (pH 7.3). Photoswitching (Fig. 1 *C* and *D* and Fig. S1 *A* and *B*) was achieved with a xenon-lamp light source (DG4; Sutter Instruments) in combination with excitation filters [445/20 nm, 379/34 nm, and 500/24 nm ("center"/"full width > 90%") and a set of neural density filters (XND; Omega Optical). The DG4 light source was coupled via liquid light guide to the back-port of the microscope to give homogeneous illumination through a LUCPlanFLN (Olympus) 0.60-N.A., 22-field number objective with a magnification of 40×, yielding an irradiance up to 500 mW/cm^2 (445 nm) at the sample stage. Dynamic intensity modulation (Fig. S1 *C* and *D*) was performed using a collimated light-emitting diode (LED) light source (470 nm; Thorlabs) coupled to the back-port of the microscope. The intensity was modulated with an analog signal from a Digidata A/D-converter (Molecular Devices).

MEA Recordings. MEA recordings were performed on wt (C57BL/6J) mice, untreated control mice, and treated *rd1* mice (fast retinal degeneration model), as well as *rd10* mice (slow degeneration model). Control mice and wt mice were used at an age >p90. Experimental mice were used 6–10 wk following AAV injection. *Rd10* mice were used at an age >6 mo. For recordings, the retina was placed ganglion cell side down (50) in the recording chamber (pMEA 100/30iR-Tpr; Multi Channel Systems) of a 60-channel MEA system with a constant vacuum pump (perforated MEA1060

system with CVP; Multi Channel Systems). A custom-made dialysis membrane weight was placed on the retina, adding positive pressure from above. Additionally, a vacuum was applied to the retina using the constant vacuum pump, adding negative pressure and improving electrode-to-tissue contact and the signal-to-noise ratio. During recording, constant perfusion of oxygenated Ames media (34 °C) was provided to the recording chamber. For *rd10* mouse retina, we supplied LAP-4 (Sigma), a group III metabotropic glutamate receptor agonist, to block any residual photoreceptor-mediated response. Comparative analysis of responses before and after drug administration was used to ensure complete blockade of photoreceptor activity at a working concentration of 20 μM. Recordings lasted between 1 and 3 h. Illumination was provided by two different light sources that were both coupled to an objective with a magnification of 4×. Light intensities were measured with a handheld power meter (Thorlabs, Inc.). A 300-W mercury arc lamp (DG-4; Sutter Instruments) with a blue bandpass filter (445/50 nm; Thorlabs, Inc.) was used for initial recordings in Fig. 2 and Fig. S2. For later recordings, an LED light source (470 nm, 24.7 mW/cm^2 or 6.3 × 10^{16} photons per cm^{-2}·s^{-1}; Thorlabs, Inc.) with a collimator lens (Thorlabs, Inc.) was used for high-frequency stimulation (Fig. 3 and Fig. S5) and for all MEA recordings in Fig. 4. Data were sampled at 25 kHz filtered between 300 and 2,000 Hz and recorded using MCS rack software (Multi Channel Systems) for offline analysis. Voltage traces were converted to spike trains offline by collecting responses using the methods described below. Spikes recorded at one electrode were sorted into single units, which we defined as "cells," via principal components analysis using Offline Sorter (Plexon). Single-unit spike clusters were exported to MATLAB (MathWorks) and were analyzed and graphed with custom software. For extracting firing rates in the dark, we averaged all bins over 3 s preceding the flash to minimize fluctuations. To extract firing rates in the light, the maximum response was taken, typically the first two bins following the flash depending on bin size (bins ranged from 20–500 ms). A cell was defined as a "responder" if the PI [(firing rate light − firing rate dark)/(firing rate light + firing rate dark)] satisfied the condition PI > 0.1 or PI < −0.1. All cells from one retina or all retinas per condition were plotted for analysis unless otherwise noted (Fig. 4 *A*–*D* showing representative traces and Fig. S5 showing "strong responders"). Two different approaches were implemented to set the threshold for spikes: (*i*) For plots showing cell-to-cell or retina-to-retina variability (Fig. 3 *C*–*H*, Figs. S3 and S4, and Table S1), the baseline for each cell was set at a threshold just above electrical noise to include all possible spikes and show the full picture, and (*ii*) for plots that show different retinas from different experiments combined, the baseline for each retina was centered at a firing rate of 10–12 Hz in the dark to allow all retinas to be plotted on a similar axis (Fig. 2 *K*–*N* and Fig. 3 *A* and *B*). Correlation matrices (Fig. 4) were constructed in MATLAB with custom software. Peristimulus time histograms of every cell were correlated with one another. The firing rates during the 1-s flash and 100 ms preceding the flash and 100 ms after the flash were used to compute the correlation matrices. Correlation values ranged between 1 and 0. A heat map was used to represent the correlation value of each data point in the matrix, with warmer colors indicating higher correlation values.

For MEA studies in dogs, a 5-mm circular patch of neuroretina centered on the area centralis was collected with a biopsy punch. A similar MEA protocol as described above was followed in one *rcd1* mutant dog (both retinas). The preparation and recording of the second *rcd1* dog retina differed slightly from the method described above. Following transfer into an MEA chamber (60-channel 200/30iR ITO array; ALA Scientific Instruments, Inc.), the retina was centered on the array ganglion cell side down and covered with a piece of dialysis membrane (Biotech RC Dialysis Tubing Trial Kit 20Kd Mwco; VWR) that was presoaked in Ringer's solution (119 mM NaCl, 2.5 mM KCl, 1 mM KH_2PO_4, 1.3 mM $MgCl_2$, 2.5 mM $CaCl_2$, 26.2 mM $NaHCO_3$, 20 mM D-glucose in ddH_20). A flat platinum ring (1-cm ring diameter, 1.0-mm wire diameter, 99.997%; VWR) was placed on top of the membrane to increase contact between the retina and the MEA. Oxygenated Ringer's solution equilibrated with 95% O_2/5% CO_2 was added to the chamber. The chamber was then transferred to the stage of an inverted microscope (Olympus IX51) and locked in place following installation of an MEA amplifier (MEA1060-Inv; Multi Channel Systems). The retina was first perfused with oxygenated Ringer's solution (rate of ∼3 mL/min) at RT for about 5 min, and a heating system was then turned on to maintain the solution in the chamber in the range of 35–37 °C. Recordings of RGC firing activity were done before and after a 20-min incubation of the retina in the photoswitch solution. Data were digitized at 10 kHz and stored on the computer hard drive using NI PCI-6071E DAQ board and custom software developed in LabView (National Instruments). For light stimulation, a 450-nm or 470-nm blue LED driven by a custom-designed circuit under the control of custom software developed in MATLAB was used. Light intensity was controlled by modifying the LED duty cycle or by using neutral density filters. The retina was stimulated from below the stage using an optical port and the 4× objective of the inverted microscope. Light intensities and stimulation timing accuracy were measured with a calibrated photodiode (OSI Optoelectronics). Light irradiances on the sample plane ranged from 0.43 to 75 mW/cm^2. A short pulse at the beginning of each stimulation series was used to trigger data acquisition, and the duration and timing of light stimulation events were recorded alongside regular data on one of the unused channels. A custom MATLAB code was used to retrieve, inspect, and convert the data into the 16-bit binary format compatible with Plexon Offline Sorter (Plexon, Inc.). In the Plexon Offline Sorter, data were high-pass–filtered at 200 Hz, and spikes were detected using a 4 SD threshold and separated into signals from individual cells using principal component analysis. The spikes with an interspike interval of less than 1 ms were deleted. Spike sorting results were exported from Plexon back into MATLAB for further analysis (generation of raster plots, calculation of firing rates, and kinetics analysis).

Open Field Test. The open field test was performed as described previously (16) with minor modifications (Fig. 5*A*). Briefly, a plastic tub (dimensions: length = 60 cm, width = 40 cm, height = 30 cm) was separated into a light compartment (length = 25 cm, width = 40 cm, height = 30 cm) with white walls and a dark compartment (length = 35 cm, width = 40 cm, height = 30 cm) with black walls. The light compartment was illuminated by a custom LED array (5 × 6 LEDs, 447.5-nm Rebel LED; Luxeon Star LEDs) centered over the compartment. The light intensity (7 mW/cm^2 or 1.6 × 10^{16} photons per cm^{-2}·s^{-1} at floor level) was homogeneously distributed throughout the floor. The mice were able to move around the box through a small opening (height = 5 cm, width = 10 cm) connecting the two compartments. Mice were brought into the testing room in their home cages, transferred into the testing box, and allowed to habituate to the new environment with their littermates for 45 min. Mice were placed back in their home cage and then tested individually. Mice were placed in the light compartment and were given a maximum of 3 min to discover that there is a second compartment. A 5-min trial began when they crossed into the dark compartment, and time spent in the light was recorded.

Mice that crossed the opening only once and stayed in the dark compartment for entire time were disqualified. Unlike wt mice, we noticed that untreated *rd1* mice showed signs of fear (i.e., hiding in corners, freezing even in open spaces) in the new environment and did not move readily. We reasoned that this fear would mask any light aversion effect, so we habituated the untreated *rd1* mice in the dark until they moved readily between compartments before testing. Mice injected >6 wk earlier with AAV2/2-hsyn-LiGluR or AAV2/2(4YF)-4xgrm6-LiGluR were injected intravitreally with $MAG0_{460}$ and tested 2, 4, 6, 8, and 10 d later at a light intensity of 7 mW/cm^2. Permanent records were made using a video camera (GoPro Hero3).

Forced Two-Choice Water Maze Task. The water maze task was performed using the protocol described by Wong and Brown (38) with minor modifications. A radial arm maze was modified into a forced two-choice task by blocking two of the five arms of the maze (Fig. 5*E*) and adding a divider (dimensions: 25 cm × 25 cm) to separate the two potential "escape arms." Two custom-built LED arrays (5 × 6 LEDs, 447.5-nm Rebel LED) were placed at the end of each escape arm. The light intensities at the release site (2 mW/cm^2 or 4.4 × 10^{15} photons per cm^{-2}·s^{-1}) and at the divider (5 mW/cm^2 or 1.1 × 10^{16} photons per cm^{-2}·s^{-1}) were measured at the water level using a handheld power meter (Thorlabs, Inc.). The LED array that cued the escape platform was triggered with square pulses to flash at 2 Hz using a stimulus generator (Stanford Research Systems).

The room was kept dark for the entire time of the experiment. Permanent records were made using a videocamera (GoPro Hero3) positioned in the center above the maze. On the day before the start of an 8-d trial, mice were habituated to the maze. Mice were placed onto the platform for 1 min. They were then released at increasing distances from the platform, and they were finally released from the chute for 10 trials. The same was repeated with the platform on the opposite side. Additionally, each day before the experiment, mice received a short habituation. They were placed onto the platform for 1 min on both sides and returned to the cages. For each trial, mice were removed from their cage, placed in a glass beaker (6-cm diameter), and then slowly (10–60 s) lowered into the water at the arm opposite of the divider. Each mouse was given a maximum of 60 s to find the platform. Trials in which mice found the hidden platform without entering the alternative arm first were counted as correct trials. Trials in which mice explored the alternative arm first or took longer than 60 s to find the platform were counted as failed trials. After the trial, mice were dried and placed into a warm chamber with a space heater and allowed to rest for at least 3 min before the next trial. All mice performed 10 trials per session with two sessions a day, with a total of 20 trials per mouse per day for 8

consecutive days. The platform and the flashing LED were moved between trials according to the following pattern: LRRLRLLLRLR and RLLRLRRLRL on alternating days. Mice that received a $MAG0_{460}$ or sham (PBS) injection were allowed to rest for >24 h afterward to avoid masking effects from anesthesia.

Statistical Analysis. The Student's' *t* test was used for statistical analysis of in vivo mouse physiology. Paired *t* tests were used for comparisons within the same group of mice before and after $MAG0_{460}$ treatment (Fig. 5 *C* and *F* and Fig. S7). Multiple *t* tests were corrected for type I errors using the Bonferroni correction.

ACKNOWLEDGMENTS. We thank Botond Roska and Connie Cepko for the 4xgrm6 promoter for ON-BC–specific expression; Lucas Pinto, Drew Friedman, and Gautam Agarwal for help with data analysis and design of custom MATLAB software; Jerome Lecoq and Adam Hoagland for design and construction of custom LEDs for mouse behavior; Meike Visel for packaging the AAVs; Ivan Tochitsky, Aaron Hamby, and Ken Greenberg for help with MEA studies; and Dr. S. Iwabe, Dr. J. M. Guzman, Ms. Kendra Rhodes, Ms. K. Carlisle, and the Retinal Disease Studies facility for clinical support with the canine studies. This work was funded by NIH/NEI Grants PN2EY01824 (of the NIH Nanomedicine Development Center for the Optical Control of Biological Function), EY06855, P30EY-001583, and by the Foundation Fighting Blindness.

1. Shintani K, Shechtman DL, Gurwood AS (2009) Review and update: Current treatment trends for patients with retinitis pigmentosa. *Optometry* 80(7):384–401.
2. Marc RE, Jones BW, Watt CB, Strettoi E (2003) Neural remodeling in retinal degeneration. *Prog Retin Eye Res* 22(5):607–655.
3. Léveillard T, Sahel JA (2010) Rod-derived cone viability factor for treating blinding diseases: From clinic to redox signaling. *Sci Transl Med* 2(26):26ps16.
4. Mazzoni F, Novelli E, Strettoi E (2008) Retinal ganglion cells survive and maintain normal dendritic morphology in a mouse model of inherited photoreceptor degeneration. *J Neurosci* 28(52):14282–14292.
5. Haverkamp S, et al. (2006) Synaptic plasticity in CNGA3(-/-) mice: Cone bipolar cells react on the missing cone input and form ectopic synapses with rods. *J Neurosci* 26(19):5248–5255.
6. Zrenner E, et al. (2011) Subretinal electronic chips allow blind patients to read letters and combine them to words. *Proc Biol Sci* 278(1711):1489–1497.
7. Mandel Y, et al. (2013) Cortical responses elicited by photovoltaic subretinal prostheses exhibit similarities to visually evoked potentials. *Nat Commun* 4:1980.
8. Humayun MS, et al.; Argus II Study Group (2012) Interim results from the international trial of Second Sight's visual prosthesis. *Ophthalmology* 119(4):779–788.
9. Twyford P, Cai C, Fried S (2014) Differential responses to high-frequency electrical stimulation in ON and OFF retinal ganglion cells. *J Neural Eng* 11(2):025001.
10. Thyagarajan S, et al. (2010) Visual function in mice with photoreceptor degeneration and transgenic expression of channelrhodopsin 2 in ganglion cells. *J Neurosci* 30(26): 8745–8758.
11. Nirenberg S, Pandarinath C (2012) Retinal prosthetic strategy with the capacity to restore normal vision. *Proc Natl Acad Sci USA* 109(37):15012–15017.
12. Lagali PS, et al. (2008) Light-activated channels targeted to ON bipolar cells restore visual function in retinal degeneration. *Nat Neurosci* 11(6):667–675.
13. Doroudchi MM, et al. (2011) Virally delivered channelrhodopsin-2 safely and effectively restores visual function in multiple mouse models of blindness. *Mol Ther* 19(7):1220–1229.
14. Busskamp V, et al. (2010) Genetic reactivation of cone photoreceptors restores visual responses in retinitis pigmentosa. *Science* 329(5990):413–417.
15. Bi A, et al. (2006) Ectopic expression of a microbial-type rhodopsin restores visual responses in mice with photoreceptor degeneration. *Neuron* 50(1):23–33.
16. Lin B, Koizumi A, Tanaka N, Panda S, Masland RH (2008) Restoration of visual function in retinal degeneration mice by ectopic expression of melanopsin. *Proc Natl Acad Sci USA* 105(41):16009–16014.
17. Tochitsky I, et al. (2014) Restoring visual function to blind mice with a photoswitch that exploits electrophysiological remodeling of retinal ganglion cells. *Neuron* 81(4): 800–813.
18. Polosukhina A, et al. (2012) Photochemical restoration of visual responses in blind mice. *Neuron* 75(2):271–282.
19. Volgraf M, et al. (2006) Allosteric control of an ionotropic glutamate receptor with an optical switch. *Nat Chem Biol* 2(1):47–52.
20. Tochitsky I, et al. (2012) Optochemical control of genetically engineered neuronal nicotinic acetylcholine receptors. *Nat Chem* 4(2):105–111.
21. Sandoz G, Levitz J, Kramer RH, Isacoff EY (2012) Optical control of endogenous proteins with a photoswitchable conditional subunit reveals a role for TREK1 in GABA(B) signaling. *Neuron* 74(6):1005–1014.
22. Levitz J, et al. (2013) Optical control of metabotropic glutamate receptors. *Nat Neurosci* 16(4):507–516.
23. Caporale N, et al. (2011) LiGluR restores visual responses in rodent models of inherited blindness. *Mol Ther* 19(7):1212–1219.
24. Kienzler MA, et al. (2013) A red-shifted, fast-relaxing azobenzene photoswitch for visible light control of an ionotropic glutamate receptor. *J Am Chem Soc* 135(47):17683–17686.
25. Reiner A, Isacoff EY (2014) Tethered ligands reveal glutamate receptor desensitization depends on subunit occupancy. *Nat Chem Biol* 10(4):273–280.
26. Sancho-Pelluz J, et al. (2008) Photoreceptor cell death mechanisms in inherited retinal degeneration. *Mol Neurobiol* 38(3):253–269.
27. Marc RE, et al. (2007) Neural reprogramming in retinal degeneration. *Invest Ophthalmol Vis Sci* 48(7):3364–3371.
28. Mandell JW, Czernik AJ, De Camilli P, Greengard P, Townes-Anderson E (1992) Differential expression of synapsins I and II among rat retinal synapses. *J Neurosci* 12(5): 1736–1749.
29. Petrs-Silva H, et al. (2011) Novel properties of tyrosine-mutant AAV2 vectors in the mouse retina. *Mol Ther* 19(2):293–301.
30. Masu M, et al. (1995) Specific deficit of the ON response in visual transmission by targeted disruption of the mGluR6 gene. *Cell* 80(5):757–765.
31. Roska B, Busskamp V, Sahel JA, Picaud S (2013) [Retinitis pigmentosa: Eye sight restoration by optogenetic therapy]. *Biol Aujourdhui* 207(2):109–121.
32. Busskamp V, Roska B (2011) Optogenetic approaches to restoring visual function in retinitis pigmentosa. *Curr Opin Neurobiol* 21(6):942–946.
33. Busskamp V, Picaud S, Sahel JA, Roska B (2012) Optogenetic therapy for retinitis pigmentosa. *Gene Ther* 19(2):169–175.
34. Rockhill RL, Daly FJ, MacNeil MA, Brown SP, Masland RH (2002) The diversity of ganglion cells in a mammalian retina. *J Neurosci* 22(9):3831–3843.
35. Kong JH, Fish DR, Rockhill RL, Masland RH (2005) Diversity of ganglion cells in the mouse retina: Unsupervised morphological classification and its limits. *J Comp Neurol* 489(3):293–310.
36. Gargini C, Terzibasi E, Mazzoni F, Strettoi E (2007) Retinal organization in the retinal degeneration 10 (rd10) mutant mouse: A morphological and ERG study. *J Comp Neurol* 500(2):222–238.
37. Bourin M, Hascoët M (2003) The mouse light/dark box test. *Eur J Pharmacol* 463(1-3): 55–65.
38. Wong AA, Brown RE (2006) Visual detection, pattern discrimination and visual acuity in 14 strains of mice. *Genes Brain Behav* 5(5):389–403.
39. Beltran WA (2009) The use of canine models of inherited retinal degeneration to test novel therapeutic approaches. *Vet Ophthalmol* 12(3):192–204.
40. Beltran WA, et al. (2014) Canine retina has a primate fovea-like bouquet of cone photoreceptors which is affected by inherited macular degenerations. *PLoS ONE* 9(3): e90390.
41. Gorostiza P, et al. (2007) Mechanisms of photoswitch conjugation and light activation of an ionotropic glutamate receptor. *Proc Natl Acad Sci USA* 104(26):10865–10870.
42. Wässle H, Puller C, Müller F, Haverkamp S (2009) Cone contacts, mosaics, and territories of bipolar cells in the mouse retina. *J Neurosci* 29(1):106–117.
43. Jacobs AL, Werblin FS (1998) Spatiotemporal patterns at the retinal output. *J Neurophysiol* 80(1):447–451.
44. Ray K, Baldwin VJ, Acland GM, Blanton SH, Aguirre GD (1994) Cosegregation of codon 807 mutation of the canine rod cGMP phosphodiesterase beta gene and rcd1. *Invest Ophthalmol Vis Sci* 35(13):4291–4299.
45. Buyukmihci N, Aguirre G, Marshall J (1980) Retinal degenerations in the dog. II. Development of the retina in rod-cone dysplasia. *Exp Eye Res* 30(5):575–591.
46. Committee on Care and Use of Laboratory Animals (1996) *Guide for the Care and Use of Laboratory Animals* (Natl Inst Health, Bethesda), DHHS Publ No (NIH) 85-23.
47. Suber ML, et al. (1993) Irish setter dogs affected with rod/cone dysplasia contain a nonsense mutation in the rod cGMP phosphodiesterase beta-subunit gene. *Proc Natl Acad Sci USA* 90(9):3968–3972.
48. Grieger JC, Choi VW, Samulski RJ (2006) Production and characterization of adeno-associated viral vectors. *Nat Protoc* 1(3):1412–1428.
49. Reiner A, Isacoff EY (2014) Photoswitching of cell surface receptors using tethered ligands. *Photoswitching Proteins*, ed Sidney C (Springer, Cambridge, NY), Vol 1148.
50. Roska B, Molnar A, Werblin FS (2006) Parallel processing in retinal ganglion cells: how integration of space-time patterns of excitation and inhibition form the spiking output. *J Neurophysiol* 95(6):3810–3822.